Desalination and Water Treatment
www.deswater.com

doi: 10.5004/dwt.2020.26187

202 (2020) 150–168
October

Permeate flux enhancement with a helical wired concentric tube in air gap membrane distillation systems

Chii-Dong Ho[a,*], Luke Chen[b], Kun-Yi Wu[a], Chi-Hsiang Ni[a], Thiam Leng Chew[c,d]

[a]*Department of Chemical and Materials Engineering, Tamkang University, Tamsui, New Taipei, Taiwan, Tel. +886-2-26215656-2724; email: cdho@mail.tku.edu.tw (C.-D. Ho)*
[b]*Department of Water Resources and Environmental Engineering, Tamkang University, Tamsui, New Taipei, Taiwan*
[c]*Department of Chemical Engineering, Faculty of Engineering, Universiti Teknologi Petronas, 32610 Seri Iskandar, Perak Darul Ridzuan, Malaysia*
[d]*CO_2 Research Center (CO2RES), Institute of Contaminant Management, Universiti Teknologi Petronas, 32610 Seri Iskandar, Perak Darul Ridzuan, Malaysia*

Received 25 October 2019; Accepted 29 May 2020

ABSTRACT

Temperature polarization plays an important role in determining the permeate flux of the membrane distillation in an air gap membrane distillation (AGMD) module. This study aimed to increase the pure water productivity of saline water desalination by applying helical wire on the circumference of a concentric-tube AGMD module to reduce the temperature polarization occurring on the smooth annulus tube of an AGMD module with a normal concentric-tube. Modeling equations of heat and mass transfer in the new design of the AGMD device with helical wire winding on the annulus of a concentric tube have been investigated theoretically and experimentally. The mathematical model proposed in this study was used to correlate a simplified equation for estimating the heat transfer coefficient and to predict the permeate flux accordingly. The effects of various operation parameters, including the feed saline water temperature, feed volumetric flow rate, air gap thickness, and helical wire pitch, on the pure water productivity were also delineated. The permeate flux enhancement for helical wire in the AGMD module could provide the maximum relative increment of up to 31.1%. The temperature polarization coefficient found in this study is ranging from 0.5527 to 0.5451 for different hot feed temperature and flow rate, respectively. An optimal helical wire module was assessed when considering both permeate flux enhancement and energy utilization effectiveness.

Keywords: Helical wired annulus; Desalination; Concentric-tube AGMD; Permeate flux enhancement

1. Introduction

Membrane distillation (MD) was developed for producing high purity water. In the process, salt impurities are removed from seawater because only water vapor molecules are transported across porous hydrophobic membranes; as a result, pure water is produced from aqueous [1,2]. The water vapor penetrates through the membrane due to the vapor pressure difference acting as a driving force across the membrane, and it then condenses on the cold side of the membrane surface [3]. Potential applications of membrane distillation have advantages for versatile separation technologies based on vaporization because of its simplicity and low operating cost, and it is considered a thermally-driven process that has been discussed by a number of researchers [4,5]. The advantage of the MD module is that it can be operated in a relatively low temperature and low-pressure stream driven by low-grade heat, such as the utilization of

* Corresponding author.

waste heat from industrial processes or the heat generated from renewable energy sources [6–8].

To improve the MD performance, namely the permeate flux and energy or thermal efficiency of the MD system, previous studies tried to find how the membrane material, the configuration of the MD module, and the operation parameters on MD performance. Both organic and inorganic membrane materials are considered before. The organic materials are polymers types such as polytetrafluoroethylene (PTFE) and polyvinylidene fluoride, while ceramics membrane was the typical inorganic material other than new materials such as graphene nanofiber [9]. Despite the permeate flux performance, the significant difference in heat conductivity between organic and inorganic membrane materials reveals an obvious difference in their thermal efficiency. Other than the membrane materials, the membrane specifications such as pore size, porosity, and thickness on membrane performance were thoroughly tested before [10]. To manufacture specific morphological characteristics of the membrane in the rendering process for improving MD performance was explored [11]. Some studies compared single MD modules with multiple stage modules, where the modules were arranged in parallel, series, or mixed were compared. [12]. Many valuable factors that can improve MD performance were found in the above studies. Other than the MD system itself, scaling prevention or mitigation is the other challenge for the MD system in practical operation to reduce permeate flux degrading. How the mechanical and chemical properties of the membrane may affect to lessen scaling or to endure scaling or fouling cleaning in the membrane were investigated [13].

The configuration of the MD system such as direct contact MD (DCMD), air gap MD(AGMD), sweep gas MD (SGMD), and vacuum MD (VMD) were broadly explored before in comparing MD performance for various MD configurations and operational parameters. Among them, air gap membrane distillation (AGMD) has been found to be one of the most energy-efficient MD devices among different types of MD modules [14] according to the MD technique proposed by Findley [15]. A flat sheet AGMD module [16] was adopted firstly, followed by spiral-wound [17] and hollow fiber [18,19] AGMD modules for desalination, which were developed to improve the permeate flux. In AGMD system, a major heat resistance occurs at the air gap because of the low heat conductivity of air. Many studies tried to improve heat transfer by adjusting the width of the gas gap [12]. An innovative design of water gap MD (WGMD) or liquid gap MD (LGMD) system was proposed to pass the gap with distilled water, and the system was found to be able to improve MD performance both in permeate flux and thermal efficiency significantly [10,12,20]. The other major heat resistance occurs on the boundary layer of the hot feed side of the membrane. The high heat loss creates a temperature gradient inside the boundary layers of both membrane surfaces in the evaporator and the condenser channels [21], resulting in the decrement of trans-membrane mass flux [22,23] due to the temperature polarization effect. The temperature polarization decreases the bulk stream temperature difference of both the hot feed and cold permeate streams. Although some heat recovery schemes [24] or fin arrangement in coolant plate were considered to improve MD performance [25], these improvement schemes mainly focus on the improvement on the permeate side of the membrane. Khalifa et al. [10] indicated that the effect of concentration polarization on permeate flux is much smaller than that of the temperature polarization [10], therefore how to improve heat transfer on hot feed side becomes critical to advance in enhancing AGMD system performance.

Many researches have investigated how to reduce temperature polarization with the use of eddy promoters in the feed flow channel, such as turbulent promoters [26], implementing filaments [27], tubular fin arrangement [28], and using tubular fin arrangement [29], thereby resulting in the temperature polarization being lessened and the distillate flux being enhanced. However, the distillate flux enhancement is accompanied with power energy consumption increments owing to the friction loss introduced by implementing eddy promoters in the flow channel needs more assessment. The sea water stream flowing through the annulus of a concentric-tube AGMD module with inserting a tight-fitting helical wire has proved to enhance the device performance [30]. Inspired by this, a new design with helical wired concentric-tube AGMD module was developed theoretically and experimentally for investigating an AGMD module that improves distillate flux with acceptable energy efficiency.

In this study, the permeate enhancement of the helical wired concentric-tube AGMD module was predicted using a theoretical model and validated with experimental data. Correlated expression of the heat transfer coefficient as referred to Reynolds number was developed utilizing the experimental results and the theoretical model. The effects of the helical wire pitch and the operation conditions on the distillate flux, as well as the ratio of distillate flux enhancement with energy consumption increment, were also analyzed for the trade-off assessment between AGMD performance enhancement and the corresponding increase in energy consumption.

2. Theoretical model

A concentric-tube AGMD module with a helical wire winding on the shell side was constructed to conduct concurrent operations to improve the distillate flux of pure water, as shown in Fig. 1. Two types of the helical wire pitch were tested, and a comparison of the performance for both modules with the helical wire channel and the empty channel was made. A mathematical model was developed considering both heat and mass transfer mechanisms to analyze the vapor molecules transported through porous hydrophobic membranes and to compare the pure water productivity in the AGMD module with and without helical wire. The mass transfer occurred in the porous membrane and air gap channel, while the heat transfer also took place in hot feed saline water, membrane, air gap, cooling plate, and cold water among the distillation process, as shown in Fig. 2. The theoretical analysis was performed based on the following assumptions [31,32]: (1) under normal atmosphere pressure; (2) a hydrophobic membrane; (3) no capillary condensation inside the pore of the membrane; (4) no reaction between the saline and the membrane; (5) no effect of the saline composition on the saturated vapor pressure;

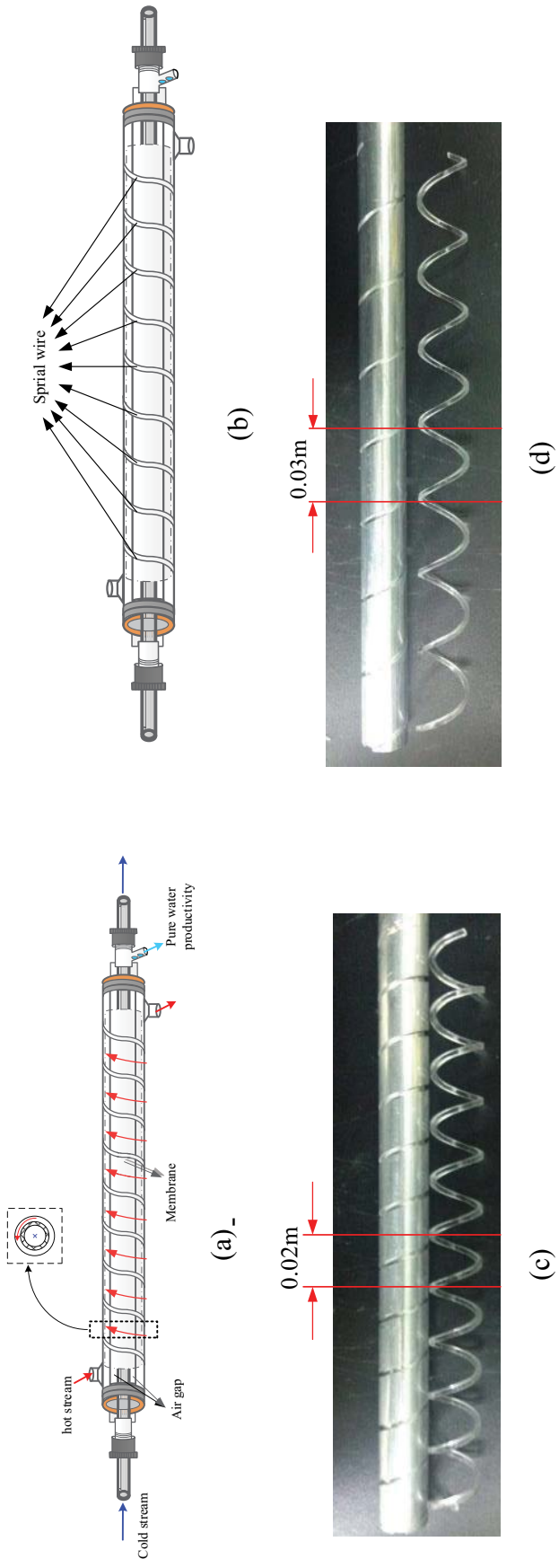

Fig. 1. Components and configuration of the AGMD module with helical wire annulus. (a) Concurrent-flow operations, (b) concentric-tube with helical wired concentric-tube, (c) 0.02 m pitch, and (d) 0.03 m pitch.

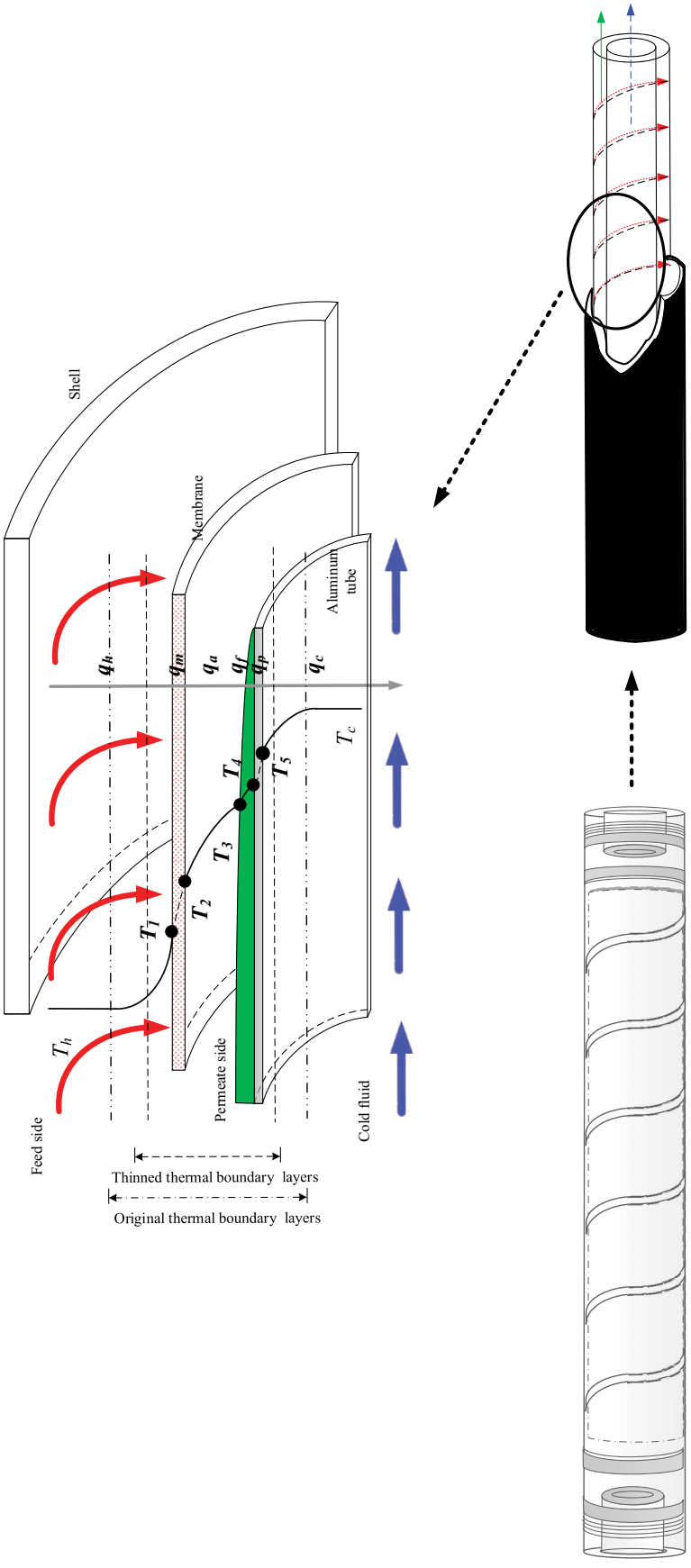

Fig. 2. Schematic temperature profile and thermal boundary layers of the AGMD module with helical wired concentric-tube.

(6) constant physical properties of the fluid, plates, and membrane; and (h) stagnant air within the membrane pore.

2.1. Heat transfer

The non-isothermal process in the AGMD system created a temperature difference across the whole module, resulting in heat and mass transfer, and thus producing pure water. The heat transfer model considered the energy balance of the enthalpy flow in each heat transfer region for (1) the hot feed stream; (2) the hydrophobic membrane; (3) the air gap; (4) the condensed pure water layer; (5) the cooling plate; and (6) cooling water under a steady-state operation, as shown in Fig. 3a. The energy balance equations of the model in each region are depicted as follows:
In the hot feed saline stream region:

$$q_h'' = h_h\left(T_h - T_1\right) \tag{1}$$

At the membrane:

$$q_m'' = \frac{k_m}{\delta_m}\left(T_1 - T_2\right) + N''\lambda \tag{2}$$

Inside the air gap:

$$q_a'' = \frac{k_a}{\delta_a}\left(T_2 - T_3\right) + N''\lambda \tag{3}$$

In the condensed water layer with the heat transfer coefficient for the condensate film [33]:

$$q_f'' = h_f\left(T_3 - T_4\right) = 0.943\left[\frac{\rho^2 g\lambda k_f^3}{\mu L\left(T_3 - T_4\right)}\right]^{1/4}\left(T_3 - T_4\right) \tag{4}$$

At the condensing plate:

$$q_p'' = \frac{k_p}{\delta_p}\left(T_4 - T_5\right) \tag{5}$$

In the cooling water:

$$q_c'' = h_c\left(T_5 - T_c\right) \tag{6}$$

Since the curvature of the concentric tube was comparatively larger than the small thickness of the annulus, the heat transfer behavior in the helical wired channel was approximate to the heat transfer in a straight flat channel. Because of the miniature size of the annular spacing as compared with the tube diameters, can be approximated as that of a parallel flat plate column inclined on edge, as confirmed by the solution with the geometry of this construction [34,35]. A one-dimensional modeling equation was obtained for the heat flux continuity, assuming well insulation on the bottom and edge sides of the modules, thus:

$$q_h'' = q_m'' = q_a'' = q_f'' = q_p'' = q_c'' \tag{7}$$

The following equations were used to describe the energy balances of the hot feed stream channel and the cold stream channel:

$$\frac{dT_h}{dz} = \frac{-W_h q}{\dot{m}C_{p,h}} \tag{8}$$

$$\frac{dT_c}{dz} = \frac{W_c q}{\dot{m}C_{p,c}} \tag{9}$$

where z is the coordinate in the flow direction and W_h and W_c represent the width of the hot and cold channel, respectively.

2.2. Mass transfer

The mass transfer flux was determined considering the mass transfer resistances in series of both the membrane and the air gap while neglecting the resistances in other layers, as shown in Fig. 3b. The permeate flux of the water vapor was estimated using membrane permeation coefficient c_m [36] and the transmembrane saturation vapor pressure difference ΔP as the driving force; hence, the amount of permeate flux that passed through the membrane pores could be expressed as:

$$N_m'' = c_m\Delta P = c_m\left(P_1^{\text{sat}} - P_2^{\text{sat}}\right) \tag{10}$$

Eq. (10) depicts the saturation vapor pressure difference due to the temperature gradient on both membrane surfaces resulting in the permeate transport across the membrane, where P_1^{sat} and P_2^{sat} are the saturated pressure of water vapor calculated using the Antoine equation on the membrane surfaces in the hot saline stream and in the air gap respectively. Hence, the permeate diffused through the air gap and reached to the cooling plate, where the collected water could condensate.

For non-volatile solutes in a lower saturation vapor pressure ($x_{\text{NaCl}} < 0.097$), the water activity coefficient a_w was calculating using the following correlation [37]:

$$a_w = 1 - 0.5x_{\text{NaCl}} - 10x_{\text{NaCl}}^2 \tag{11}$$

Hence, the saturated water vapor pressure on the membrane surface of the feed saline stream side P_1^{sat} could be expressed as:

$$P_1^{\text{sat}} = x_w a_w P_w^{\text{sat}} \tag{12}$$

where x_w is the mole fraction of the water vapor and P_w^{sat} is the total saturation of the vapor pressure, respectively. The amount of molar vapor flux diffusing through a stagnant air film over the air gap layer by molecular diffusion [38] was expressed as:

$$N_a'' = c_a\left(P_2^{\text{sat}} - P_3^{\text{sat}}\right) \tag{13}$$

The overall water production was then calculated by equating the permeate fluxes in the membrane and the air

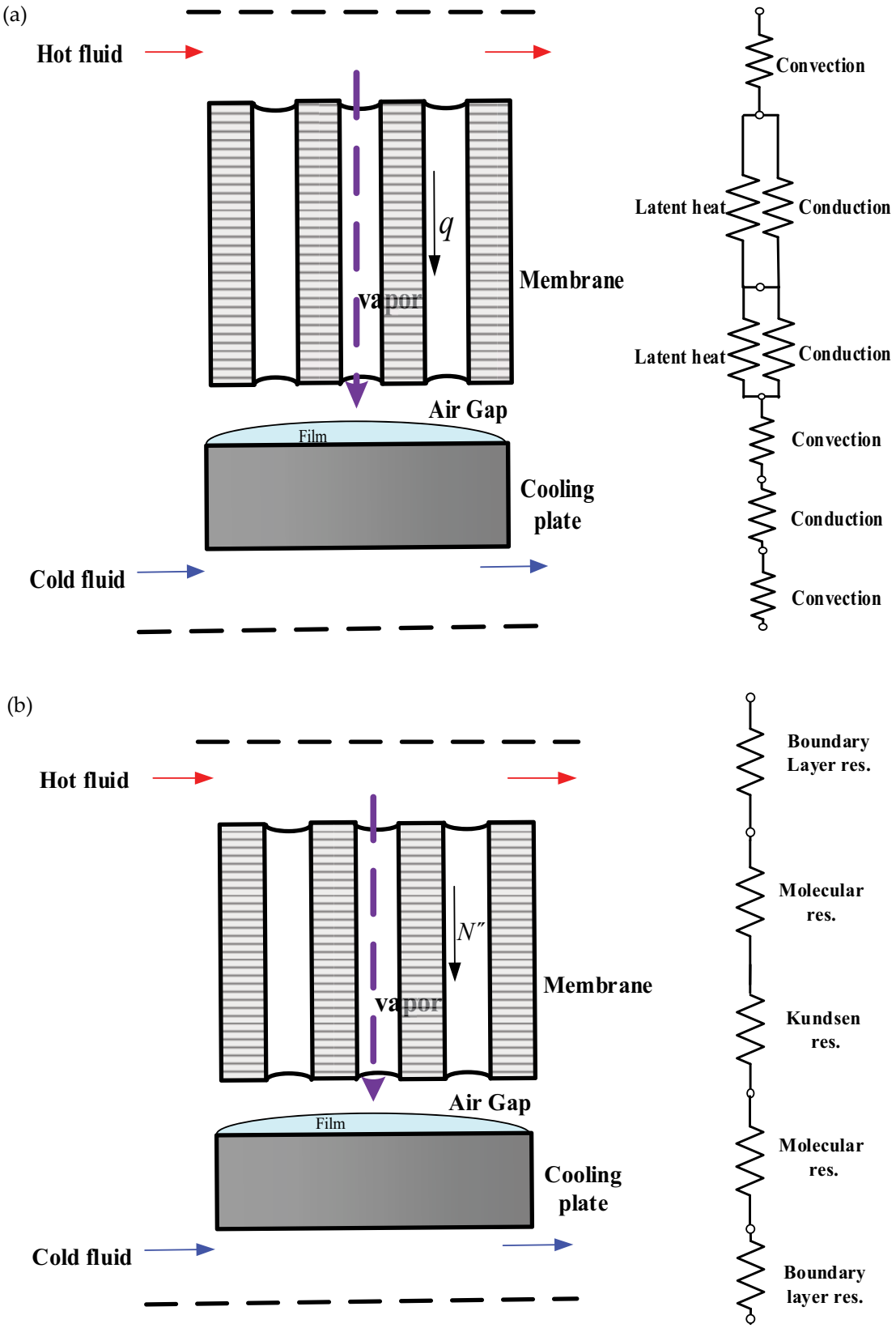

Fig. 3. (a) Heat transfer resistances models across the AGMD module and (b) mass transfer resistances models across the AGMD module.

gap, as expressed in Eqs. (2) and (3), with the total mass-transfer resistances:

$$N_a'' = N_m'' = c_T\left(P_1 - P_3\right) = c_T \left.\frac{dP}{dT}\right|_{T_{\text{avg}}} \left(T_1 - T_3\right) = c_T \frac{P_{\text{avg}} \lambda M_w}{RT_{\text{avg}}^2}\left(T_1 - T_3\right) \tag{14}$$

Where the overall mass transfer coefficient c_T is expressed as:

$$c_T = \left(\frac{1}{c_m} + \frac{1}{c_a}\right)^{-1} \tag{15}$$

2.3. Temperature polarization

The temperature polarization coefficient (TPC) [39] is an indicator used to evaluate thermal performance for an AGMD configuration and is defined as the ratio of the temperature difference at the membrane surfaces to the temperature difference of the bulk temperatures:

$$\text{TPC} = \tau_{\text{temp}} = \frac{T_1 - T_3}{T_h - T_c} \tag{16}$$

Temperature polarization in a membrane distillation system is inevitable, but it could be improved by applying helical wire on the circumference of the concentric tube of a hot feed channel as an eddy promoter to enhance the heat transfer. The combinations of each heat flux term from Eqs. (2), (3), (4)–(6) led to the overall heat transfer coefficient of the hot feed stream and cooling stream, respectively:

$$q_{\text{ma}}'' = q_{\text{cond.}}'' + q_{\text{vap.}}'' = \left\{\left(\frac{k_m}{\delta_m} + \frac{k_a}{\delta_a}\right)^{-1} + \left[c_T \frac{\left(\left(1 - x_{\text{NaCl}}\right)\left(1 - 0.5x_{\text{NaCl}} - 10x_{\text{NaCl}}^2\right)P_w^{\text{sat}} + P_3^{\text{sat}}\right)\lambda^2 M_w}{2RT_{\text{avg}}^2}\right]\right\}\left(T_1 - T_3\right) = H_m\left(T_1 - T_3\right) \tag{17}$$

$$q_{fc}'' = \frac{1}{1/h_f + \delta_p/k_p + 1/h_c}\left(T_3 - T_c\right) = H_c\left(T_3 - T_c\right) \tag{18}$$

Manipulating and solving Eqs. (17) and (18) with the aid of Eq. (1) yielded:

$$T_h = T_1 + \frac{H_m}{h_h}\left(T_1 - T_3\right) \tag{19a}$$

$$T_c = T_3 - \frac{H_m}{H_c}\left(T_1 - T_3\right) \tag{19b}$$

or

$$T_1 = \frac{h_h T_h + H_m T_3}{h_h + H_m} \tag{20a}$$

$$T_3 = \frac{H_c T_c + H_m T_1}{H_c + H_m} \tag{20b}$$

Substituting Eqs. (20a) and (20b) into (16) resulted in the TPC:

$$\tau_{\text{temp}} = \frac{h_h H_c}{h_h H_c + h_h H_m + H_c H_m} \tag{21}$$

Therefore, the governing equations of the hot feed and cold stream channels expressed in Eqs. (8) and (9) could be rewritten in terms of the τ_{temp} coefficients as:

$$\frac{dT_h}{dz} = \frac{-W}{\dot{m}C_{ph}} H_m \tau_{\text{temp}}\left(T_h - T_c\right) \tag{22}$$

$$\frac{dT_c}{dz} = \frac{W}{\dot{m}C_{pc}} H_m \tau_{\text{temp}}\left(T_h - T_c\right) \tag{23}$$

With the expression of T_1 and T_3 by Eqs. (20a) and (20b), the TPC τ_{temp} could be rewritten as:

$$\tau_{\text{temp}} = \frac{T_1 - T_3}{T_h - T_c} = \frac{h_h H_c}{h_h H_c + h_h H_m + H_c H_m} \tag{24}$$

τ_{temp} is commonly used to express the significance of the fluid side heat transfer resistance. A higher value of τ_{temp} represents a thinner thermal boundary layer, which results in less thermal resistance. The heat transfer across the membrane, including the latent heat associated with the vapor flux and the conductive heat transfer across the membrane, could be expressed as:

$$q_m = N_m'' \lambda + \frac{k_m}{\delta_m}\left(T_1 - T_2\right) \tag{25}$$

where $N_m'' \lambda$ is characterized as the latent heat and $\frac{k_m}{\delta_m}\left(T_1 - T_2\right)$ is the conductive heat transfer. The thermal conductivity of membrane k_m could be determined by the thermal conductivities of the vapor in membrane pore k_g and the solid membrane material k_s by [40]:

$$k_m = \varepsilon k_g + \left(1 - \varepsilon\right)k_s \tag{26}$$

Knudsen diffusion and molecular diffusion [36,41,42] were taken into account in determining the membrane permeation coefficient by considering the mean free path of the water molecules and the membrane pore size as below:

$$c_m = \left(\frac{1}{c_K} + \frac{1}{c_M}\right)^{-1} = \left\{\left[1.064\frac{\varepsilon r}{\tau\delta_m}\left(\frac{M_w}{RT_m}\right)^{1/2}\right]^{-1} + \left[\frac{1}{|Y_m|_{\ln}}\frac{D_m\varepsilon}{\delta_m\tau}\frac{M_w}{RT_m}\right]^{-1}\right\}^{-1} \quad (27)$$

The tortuosity τ could be estimated using the porosity of the membrane [42]:

$$\tau = \frac{1}{\varepsilon} \quad (28)$$

2.4. Numerical scheme

The temperature distributions of the hot feed stream, cold stream, and membrane surfaces along the flowing direction of the module were obtained by solving Eqs. (22) and (23) numerically using the fourth-order Runge–Kutta method, and then the permeate flux was calculated. Using the AGMD system configuration and the coordinate system shown in Fig. 4, when given the fluid properties and boundary conditions of the flow as input, the convective heat transfer coefficients were obtained by iterative procedures with the initial guess until convergence was reached. With the obtained convective heat transfer coefficients, the temperature distribution along both sides of the membrane surfaces could also be iteratively solved. The iterative procedures are illustrated in a computational flow chart, as shown in Fig. 5.

The heat transfer coefficient could be approximated using the heat transfer correlation in a flat plate channel under a laminar flow [43] while neglecting the curvature and thin annulus of the concentric-tube channel, as shown below:

$$\mathrm{Nu}_{\mathrm{laminar}} = 4.36 + \frac{0.036\,\mathrm{Re}\,\mathrm{Pr}\left(d_h / L\right)}{1 + 0.011\left(\mathrm{Re}\,\mathrm{Pr}\left(d_h / L\right)\right)^{0.8}} \quad (29)$$

The extent of the heat transfer enhancement was expressed by an enhancement factor which was defined as the ratio of the heat transfer coefficient of the improved helical wired channel to that of an empty channel. The enhancement factor of the heat transfer coefficient for the AGMD modules was therefore defined as a Nusselt number in a helical wired channel relative to that in an empty channel:

$$\mathrm{Nu}^s = \frac{hd_h}{k} = \alpha^s \mathrm{Nu}_{\mathrm{lam}} \quad (30)$$

The Nusselt numbers of various helical wire pitches for the hot feed saline stream were correlated into five dimensionless groups according to Buckingham's π theorem:

$$\mathrm{Nu}^s = f\left(\frac{L_h}{d_h}, \frac{L_c}{d_h}, \mathrm{Re}, \mathrm{Pr}\right) \quad (31)$$

where d_h is the hydraulic diameter of the empty channel and L_h and L_c are the equivalent channel length of the hot and cold channels, respectively, as illustrated in Fig. 4.

The increment in energy consumption was inevitable due to the increased frictional loss caused by applying a helical wire on the circumference of the concentric-tube AGMD module. The energy consumption of the AGMD module, which included the head losses in both the hot feed and cold streams of the concentric-tube channels, was determined using Fanning friction factor f_F of an equivalent flat plate channel [37]:

$$H_{\mathrm{lost}} = \dot{m}_h \ell w_{f,h} + \dot{m}_c \ell w_{f,c} = Q_h \rho_h \ell w_{f,h} + Q_c \rho_c \ell w_{f,c} \quad (32)$$

$$\ell w_{f,h} = \frac{2f_{F,h}u_h^2 L}{d_{h,h}},\ \ell w_{f,c} = \frac{2f_{F,c}u_c^2 L}{d_{h,c}} \quad (33)$$

In which:

$$\overline{v}_h = \frac{Q}{D_h W_h},\ \overline{v}_c = \frac{4Q}{\pi D_c^2} \quad (34)$$

$$d_{h,h} = \frac{4D_h W_h}{2\left(D_h + W_h\right)},\ d_{h,c} = \frac{4D_c W_c}{2\left(D_c + W_c\right)} \quad (35)$$

where $\overline{v}_h$ and $\overline{v}_c$ are the average velocity in the hot feed and cold streams, d_{hh} and d_{hc} represents the hydraulic diameters in the hot feed and cold channels, respectively. D_h and D_c are diameter of the hot feed and cold channels, respectively, and W_h is the width of the helical wired channel.

The Fanning friction factor could be estimated using a correlation based on the aspect ratio of the channel [44]:

$$f_{F,h} = \frac{C}{\mathrm{Re}_h},\ f_{F,c} = \frac{C}{\mathrm{Re}_c} \quad (36)$$

$$C = 24\left(1 - 1.3553\alpha + 1.9467\alpha^2 - 1.7012\alpha^3 + 0.9564\alpha^4 - 0.2537\alpha^5\right) \quad (37)$$

The distillate flux enhancement I_N and energy consumption increment I_P were defined as below:

$$I_N = \frac{N_s'' - N_b''}{N_b''} \times 100\% \quad (38)$$

$$I_P = \frac{P_s - P_b}{P_b} \times 100\% \quad (39)$$

where the subscript s represents the helical concentric-tube channel and the subscript b represents the empty channel. The trade-off between distillate flux enhancement I_N and energy consumption increment I_P was also assessed by an indicator, which is the ratio I_N/I_P for the new design of the AGMD module.

3. Experimental setup

The experimental setup of the concentric-tube AGMD module with a helical wired channel is illustrated in Fig. 6

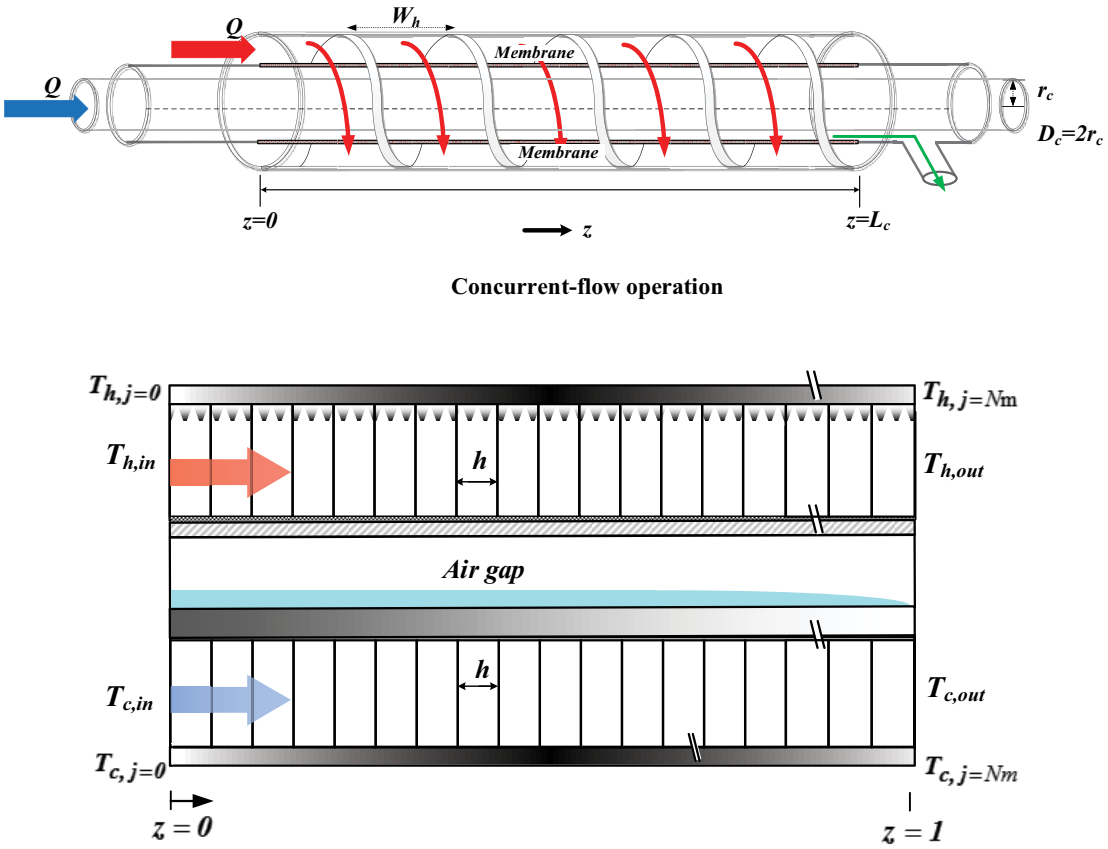

Fig. 4. Configuration and the schematic coordinates of the helical wired AGMD module.

and a photo of the present experimental device is shown in Fig. 6. The dimensions of the acrylic made helical wire are specified in Figs. 1c and d, in which the pitch of the helical wire was used as a design parameter. The pitch of 2 and 3 cm was used in this study. The detailed configuration of the concentric-tube AGMD module with a helical wired channel is illustrated in Fig. 7. The helical wire on the circumference of the concentric-tube provided a larger convective heat-transfer coefficient when compared with the empty channel because the applied helical wire could disrupt the thermal boundary layer on the hot feed stream side. Hence the heat transfer resistance was reduced, and thus, a higher permeate flux was observed.

The inlet temperature and flow rate of the hot feed were regulated for various experimental runs to compare the permeate flux of the flow channel without a helical wire and with different pitches of helical wire, while keeping the temperature and flow rate of the cold stream fixed. The amount of the produced pure water or permeate flux was then collected and measured for comparison.

The length of the concentric-tube of the AGMD module was 0.2 m and the diameter of the helical wire was 0.002 m. A hydrophobic PTFE/PP composite membrane (ADVANTEC) with a nominal pore size of 0.2 μm, a porosity of 0.72, and a thickness of 130 μm was used. The hot saline water of 3.5 wt.% NaCl was prepared using distilled water and conducted for various inlet hot saline temperatures (40°C, 45°C, 50°C, 55°C) with various flow rates (0.3, 0.5, 0.7, 0.9 L/min). The cross-sectional area of the empty channel and the helical wired channels with a pitch of 2 and 3 cm was 1.08 $m^2 \times 10^{-4}$ m^2, 4 $m^2 \times 10^{-5}$ m^2, and 6 $m^2 \times 10^{-5}$ m^2 respectively, while the cold stream had a fixed inlet temperature of 25°C and a volumetric flow rate of 0.9 L/min with a channel cross-sectional area of 3×10^{-5} m^2. Two thermostats were used to supply the hot feed saline and cold stream at specified temperatures. The distillate flux that condensed on the cold plate was then collected and weighted using an electronic balance.

4. Results and discussion

The effect of the helical wired concentric-tube AGMD module in enhancing the permeate flux and reducing energy efficiency under a concurrent-flow operation was investigated theoretically and experimentally as compared to the module of the empty channel without helical wire. The one-dimensional temperature distributions of the helical wired concentric-tube AGMD module were solved numerically with respect to the dimensionless longitudinal coordinate, say $\xi = z/L$, for the channel with a helical pitch of 2 and 3 cm and an empty channel respectively under a concurrent-flow operation, as shown in Fig. 8.

The comparison of the temperature profiles indicated no significant temperature gradient change on the membrane surface and condensed pure water surface (T_1, T_3) for the empty channel and the helical wired channel. It is noticed

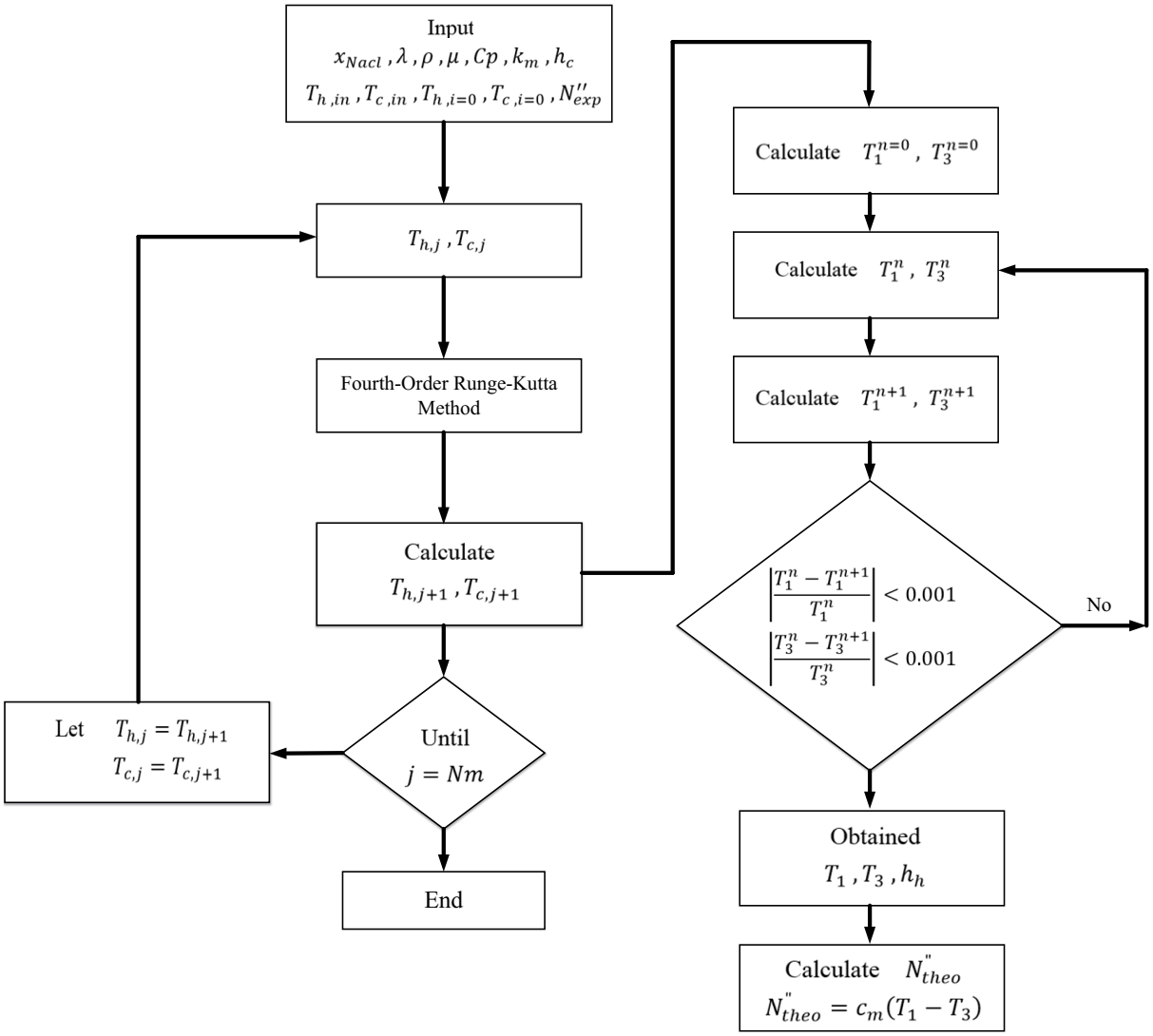

Fig. 5. Computational flow chart for the numerical scheme in predicting heat transfer and permeate flux of the AGMD module.

that an obvious temperature gradient change of the bulk flow in the hot and cold stream (T_h, T_c) was developed from the entrance to the outlet, because the helical wire enhanced the heat transfer on the bulk flow of the hot feed stream, which leads to a greater temperature drop along the channel direction when compared with the empty channel.

Higher τ_{temp} values were found for the AGMD module with the helical wire attached channel when compared to the τ_{temp} values of the AGMD module of the empty channel, as shown in Fig. 9. The helical wire could both reduce the thermal boundary layer on the membrane surface and prolong the liquid/tube contact length, and thus, a higher heat-transfer efficiency was observed and less temperature polarization was found. A comparison of the increment of τ_{temp} values for the AGMD modules revealed that the τ_{temp} values in descending order were helical wire pitches of 2 and 3 cm and the empty channel, as shown in Fig. 9. The overall permeate flux was enhanced for the AGMD module with helical wired channels more than that of the empty channel. The AGMD module wound with the narrower helical pitch (2 cm) strengthened the permeate flux more than that wound with a wider pitch (3 cm), and hence, a larger τ_{temp} value was predicted for the channel with a pitch of 2 cm than for that with a pitch of 3 cm due to a higher convective heat-transfer coefficient enhancement. The τ_{temp} of the 40°C hot feed stream was higher than that of the 55°C hot feed stream, as shown in Fig. 9. This indicated that the thermal efficiency of the 40°C feed stream was higher than that of the 55°C feed stream as explained by Khalifa et al. [10] that a hotter feed stream may compensated by heat conduction.

The theoretical predicted permeate flux N''_{theo} and the experimental permeate flux N''_{exp} were compared and the errors were summarized, as shown in Table 1. The error analysis was ranging from the maximum of 12.98% to the minimum of 1.93% and the average error between N''_{theo} and N''_{exp} was 8.14%. The correlation of the Nusselt number for the empty channel is depicted in Eq. (29), while the correlation of the Nusselt number for the helical wired channels is shown in Eq. (30). The α^S was determined via regression analysis:

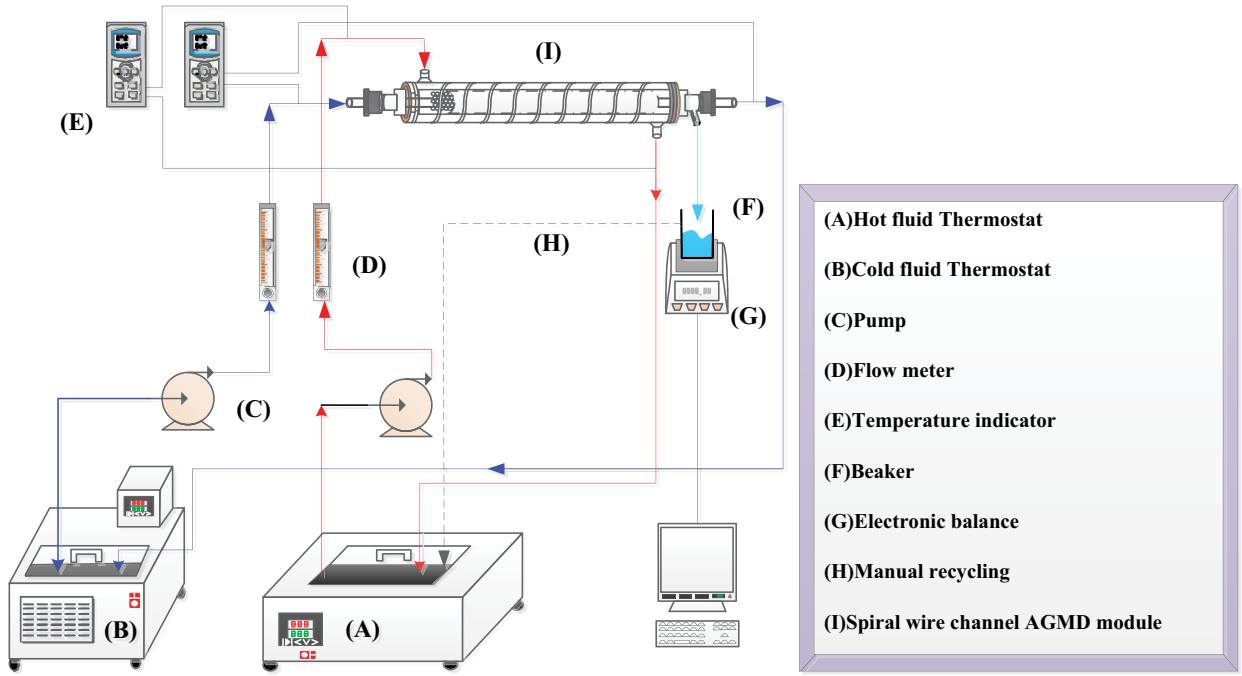

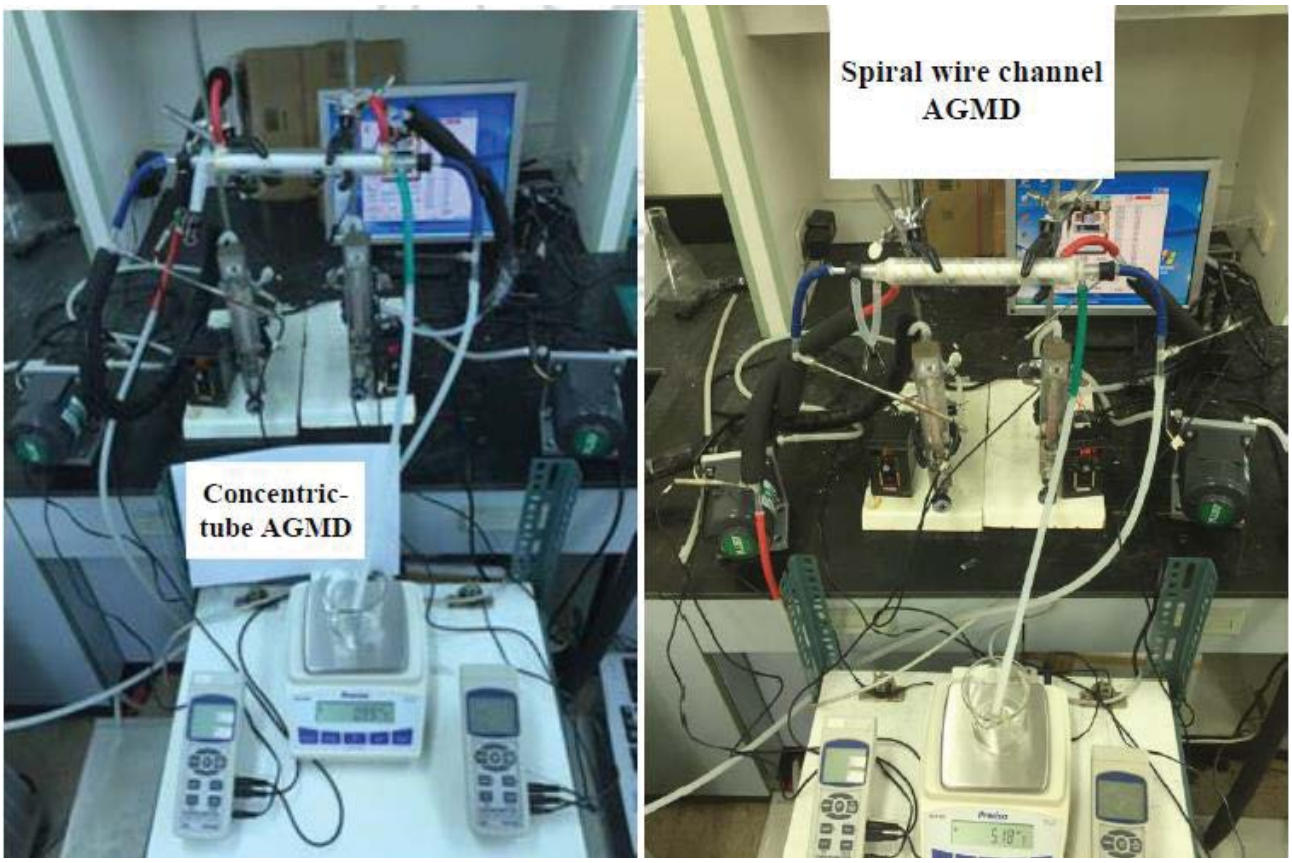

Fig. 6. Experimental setup and the photo of the helical wired concentric-tube AGMD module.

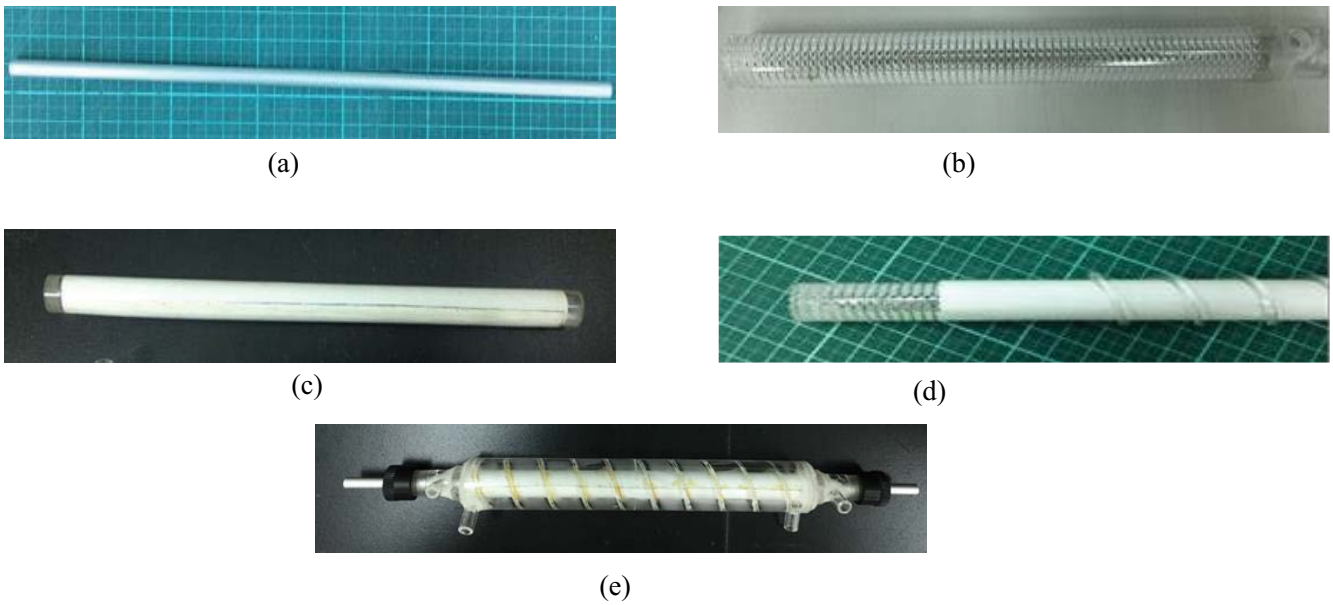

Fig. 7. Details of the material and configuration of the helical wired AGMD module. (a) Aluminum tube, (b) perforated acrylic tube, (c) membrane tube, (d) membrane tube with spiral wire, and (e) concentric tube with helical wire channel.

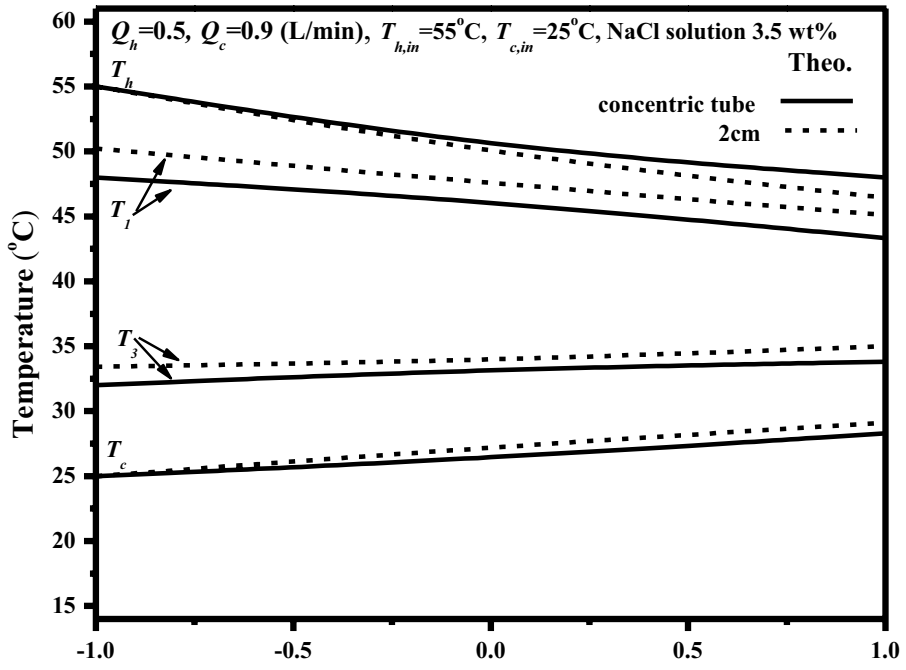

Fig. 8. Comparison of temperature distributions for the helical wired channel and empty channel.

$$\mathrm{Nu}^{s} = 0.0809947 \ln\left(\frac{L_h}{d_h}\right)^{1.835975} \mathrm{Nu}_{\mathrm{laminar}} \tag{40}$$

A review of the average error in Table 1 and the model correlation results in Fig. 10 revealed that the theoretical model could accurately predict the heat transfer coefficients for the AGMD modules with an empty channel and without helical wired channels.

The higher inlet saline temperature created a higher temperature gradient between the membrane surfaces and resulted in producing a higher permeate flux. The permeate flux increased with the increase of the volumetric flow rate, which enhanced the convective heat-transfer rate of

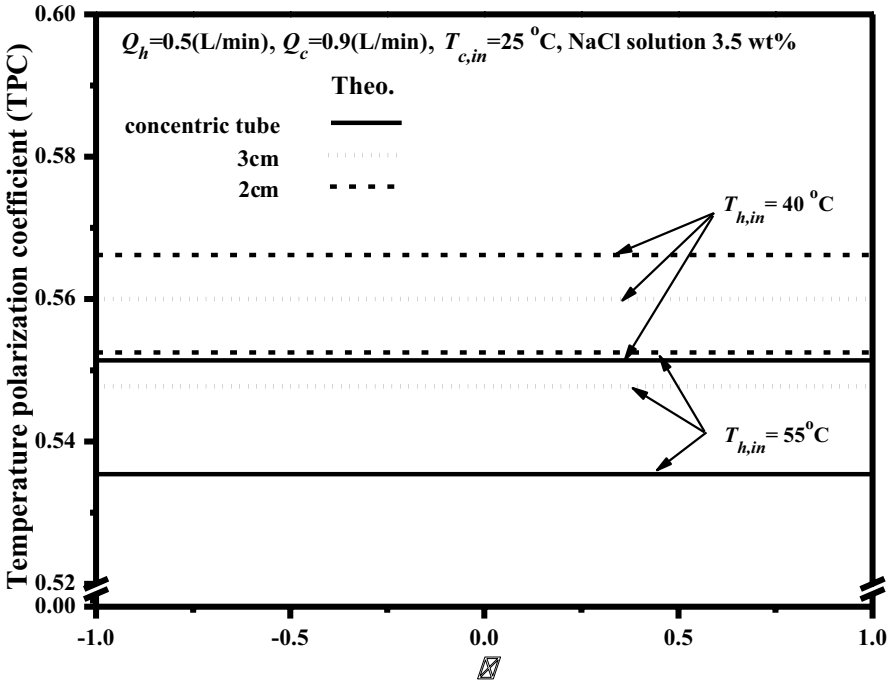

Fig. 9. Effect of the helical wire pitch and feed saline temperature on TPC.

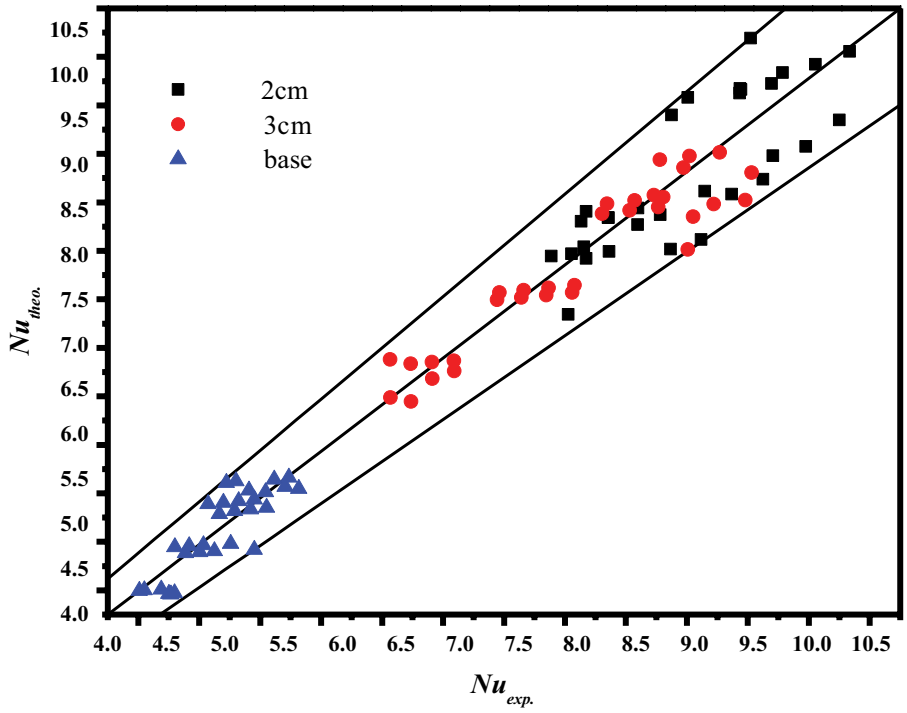

Fig. 10. Comparison of correlated and experimental Nusselt numbers.

the hot feed stream, as illustrated in Fig. 11. Meanwhile, the permeate flux enhancement for the channel with a helical wire pitch of 2 cm was more than the enhancement found in the channel with a helical wire pitch of 3 cm. A considerable improvement of permeate flux of the device with the helical wired channel as compared that in the device with the empty channel was also found in a previous study [45,46]. Though the phenomenon of heat and mass transfer behaviors in the present study could be analogized from those in our previous work [46], the manners of permeate

Table 1
Comparisons of theoretical and experimental distillate flux under concurrent-flow operation

$T_{h,in}$ (°C)	Q (L/min)	Empty channel			Helical wired channel					
					2 cm			3 cm		
		N''_{exp} (kg/m²h)	N''_{theo} (kg/m²h)	Error%	N''_{exp} (kg/m²h)	N''_{theo} (kg/m²h)	Error %	N''_{exp} (kg/m²h)	N''_{theo} (kg/m²h)	Error %
40	0.3	1.286	1.453	12.98	1.575	1.762	11.87	1.459	1.646	12.81
	0.5	1.589	1.752	10.25	1.942	2.151	10.76	1.792	2.012	12.27
	0.7	1.768	1.935	9.445	2.203	2.408	9.30	2.032	2.255	10.97
	0.8	1.878	2.052	9.265	2.396	2.602	8.59	2.235	2.421	8.32
45	0.3	1.719	1.922	11.81	2.103	2.348	11.65	1.953	2.184	11.82
	0.5	2.148	2.386	11.07	2.678	2.963	10.64	2.475	2.743	10.84
	0.7	2.387	2.599	8.883	2.984	3.276	9.78	2.761	3.047	10.35
	0.8	2.445	2.65	8.374	3.126	3.384	7.22	2.905	3.138	8.02
50	0.3	2.276	2.516	10.54	2.832	3.106	9.67	2.618	2.877	10.46
	0.5	2.821	3.072	8.897	3.531	3.824	8.29	3.235	3.535	9.27
	0.7	3.084	3.328	7.911	3.932	4.205	6.94	3.631	3.912	7.73
	0.8	3.289	3.512	6.78	4.265	4.496	5.64	3.962	4.186	5.65
55	0.3	2.759	3.024	9.604	3.445	3.761	9.17	3.146	3.461	10.01
	0.5	3.415	3.707	8.55	4.408	4.714	6.94	3.982	4.328	8.68
	0.7	3.769	4.06	7.72	5.116	5.312	4.83	4.613	4.893	6.04
	0.8	4.056	4.302	6.06	5.535	5.642	1.93	4.986	5.211	4.51

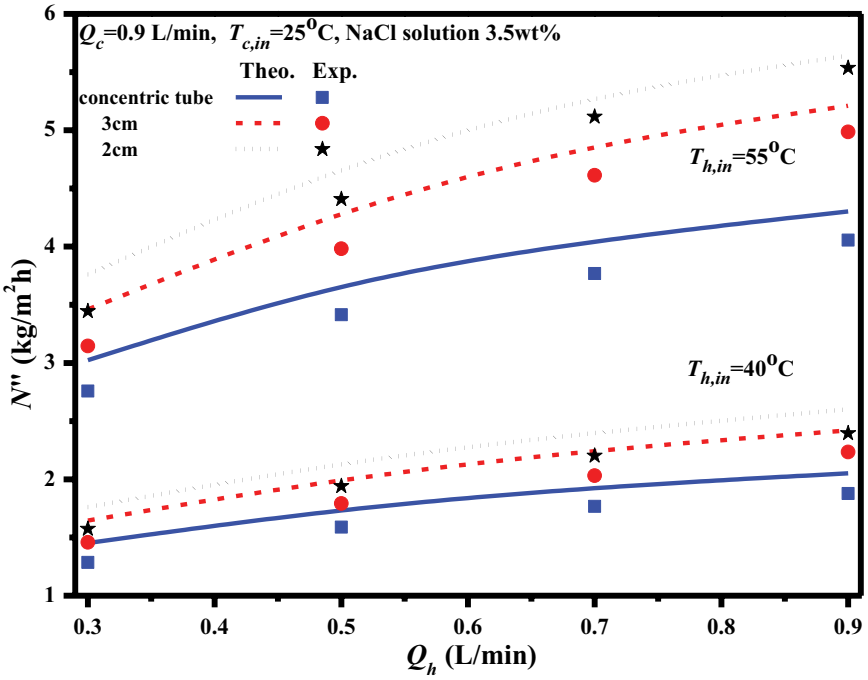

Fig. 11. Effect of the helical pitch, feed saline temperature, and flow rate on permeate flux.

flux diffusing the air gap and reaching to the cooling plate are somewhat different in transfer mechanisms. Actually, the present study is an extension of our previous work of DCMD module to apply the case of the AGMD module with a helical wired concentric-tube system.

The results showed that the helical wired channel could enhance the convective heat-transfer coefficient. Up to a 31.1% maximum distillate flux increment was found for the 55°C saline stream with feed flow rate of 0.8 L/min in a concurrent-flow operation, as listed in Table 2. The results

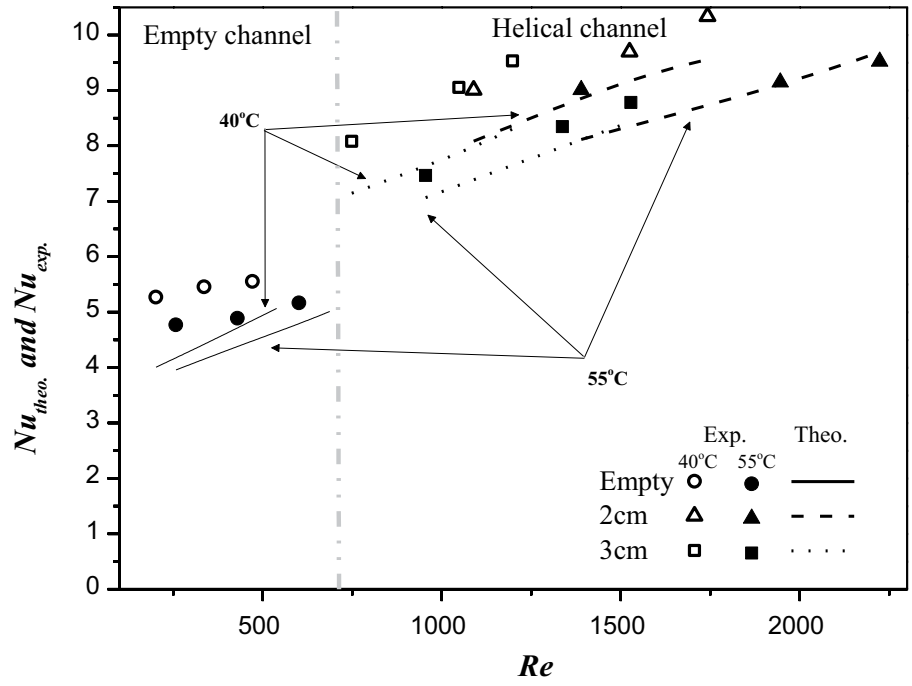

Fig. 12. Dependence of Nu and Re for the empty channel and the helical wired channels.

of how permeate flux varies with inlet hot feed temperature, volumetric flow rates, with/without helical wire, and various helical wire pitches in a concentric-tube AGMD module could be concluded as follows:

- The higher inlet saline temperature in the hot feed stream resulted in higher pure water productivity, while less τ_{temp} or less thermal efficiency was found.
- The permeate flux increased with the increase of the feed volumetric flow rate.
- The permeate flux enhancement was observed when applying helical wire on the circumference of a concentric tube where the permeate flux enhancement of the 2 cm wire pitch was higher than that of the 3 cm wire pitch.

The dependence of the Nusselt number on the Reynolds number is illustrated in Fig. 12, where the Nu number increased with the increasing Re. When comparing the theoretical predictions with the experimental results shown in Fig. 12, the predicted Nu numbers were close to the experimental results for both the empty channel and the helical wired channels. The effect of applying helical wire in a concentric tube could significantly increase the Nusselt number or convective heat-transfer coefficient in the AGMD module as compared to the module of the empty channel without helical wire. The results showed that a narrower helical wire pitch resulted in a higher Nusselt number when comparing the Nu number of wire pitches of 2 and 3 cm.

The experimental and numerical results of the permeate flux N''_{theo}, N''_{exp}, τ_{temp}, and I_N are summarized in Table 2. The permeate flux enhancement I_N for helical wire in the AGMD module with a wire pitch of 2 and 3 cm could provide the maximum relative increment of up to 31.1% and 21.1%, respectively, as compared to the permeate flux of the module with an empty channel. Based on the assumption that the solar heat source is attainable, the cost of this system was extrapolated from the cost data of AGMD with solar heat source estimated in our previous study [47]. The previous AGMD cost was estimated ranging from 15.7 to 8.54 \$/m^3 which are corresponding to the daily pure water production ranges from 100 to 200 kg/m^3. Base on a 30% permeate flux enhancement and the 135 kg/m^3 daily pure water production of this study, the cost of this MD system is estimated to be between 6.6 and 12.1 or 8.6 \$/m^3 by interpolating the cost based on the amount of daily pure water production and the increment of permeate flux enhancement.

The ratio of permeate flux enhancement and energy consumption increment I_N/I_P was calculated and presented in Fig. 13 as an indicator for assessing the optimal design of an AGMD module when considering both the permeate enhancement and energy consumption rise. The experimental results concluded that the ratio of I_N/I_P increased with increasing the flow rate and temperature of the hot feed stream and decreased with increasing the helical wire pitch. To optimize the AGMD design, it would be necessary to consider both the permeate flux enhancement and the corresponding energy consumption.

A comparison of the permeate flux enhancement parameters revealed that increasing the temperature of the hot feed stream was comparatively more effective than increasing the hot feed volumetric flow rate. The I_N/I_P ratio of the concentric-tube AGMD module with a helical wire pitch of 3 cm was higher than that of the module with a helical wire pitch of 2 cm, as shown in Fig. 13. The results showed that both the Nusselt number and the permeate flux of the helical wired concentric-tube AGMD module with a wire pitch of 2 cm

Table 2
Effect of channel designs on I_N under concurrent-flow operations

$T_{h,in}$ (°C)	Q (L/min)	Empty channel	Helical wired channel			
			2 cm		3 cm	
		N''_{theo} (kg/m²h)	N''_{theo} (kg/m²h)	I_N (%)	N''_{theo} (kg/m²h)	I_N (%)
40	0.3	1.922	2.348	22.2	2.184	13.63
	0.5	2.386	2.963	24.2	2.743	14.96
	0.7	2.599	3.276	26.04	3.047	17.23
	0.8	2.65	3.384	27.69	3.138	18.41
55	0.3	3.024	3.761	24.37	3.461	14.45
	0.5	3.707	4.714	27.16	4.328	16.75
	0.7	4.06	5.312	30.83	4.893	20.51
	0.8	4.302	5.642	31.14	5.211	21.12

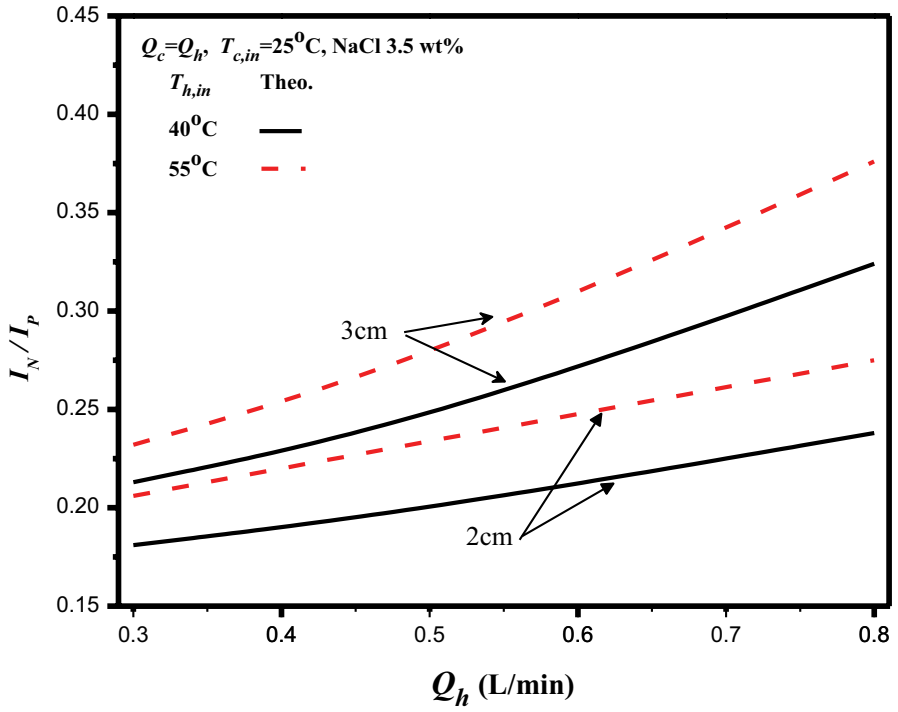

Fig. 13. Effect of the feed saline temperature, helical wire pitch, and flow rate on the I_N/I_P ratio.

were higher than those for the module with a wire pitch of 3 cm; however, its energy consumption was comparatively higher in the reverse order. Therefore, the value of the I_N/I_P ratio revealed better effective energy utilization and less power consumption when a 3 cm wire pitch in the helical concentric-tube AGMD module was applied.

5. Conclusions

Distillate flux enhancement from saline desalination was achieved by applying a helical wired concentric-tube AGMD module to reduce the thermal boundary layer and enlarge the convective heat-transfer coefficient, thereby resulting in a substantial increase in producing permeate flux. The helical wired concentric-tube AGMD system was investigated experimentally and theoretically in consideration of both the heat and mass transfer mechanism for each sub-layer of the module, and the results were validated by experimental data using various volumetric flow rates, feed saline temperatures, and helical wire pitches as parameters. The mathematical modeling was developed theoretically and solved numerically to predict the temperature distribution, distillate flux, and energy consumption. The experimental works demonstrated the model's technical feasibility, and an average permeate flux enhancement of up to 26.7% was achieved for a 55°C saline feed flow rate of 0.8 L/min with a helical wire pitch of 2 cm. A correlated expression of the heat-transfer enhancement

factor was also obtained from the experimental results of the helical wired channels. The permeate flux enhancement for helical wire in the AGMD module with a wire pitch of 2 and 3 cm could provide the maximum relative increment of up to 31.1% and 21.1%, respectively, as compared to the permeate flux of the module with an empty channel. The TPC τ_{temp} found in this study is ranging from 0.553 to 0.545 for hot feed temperature of 40°C to 55°C and the flow rate of 0.5 to 0.8 L/min, respectively.

The theoretical predictions and experimental results showed that increasing the saline feed temperature and volumetric flow rate enhanced the distillate flux, while the flow channel with a narrower helical wire pitch resulted in a higher distillate flux. A comparison of the permeate flux enhancement parameters revealed that increasing the temperature of the hot feed stream was comparatively more effective than increasing the hot feed volumetric flow rate. Both the Nusselt number and the permeate flux of the helical wired concentric-tube AGMD module with a wire pitch of 2 cm were higher than those of the module with a wire pitch of 3 cm; however, the energy consumption was comparatively higher in the reverse order. The module with a helical pitch of 3 cm was more energy efficient than the module with a helical wire pitch of 2 cm, while both the distillate flux enhancement and energy consumption increment were taken into account. To improve the heat transfer on both hot feed and permeate sides of a membrane by integrating the current helical module with schemes proposed by previous studies can be further explored.

Symbols

a_w	—	The water activity coefficient
C_p	—	Heat capacity, (J/(kg K)
c_M	—	Membrane coefficient based on the molecular diffusion model, kg/(m² Pa h)
c_T	—	Total mass transfer coefficient, kg/(m² Pa h)
c_a	—	Mass transfer coefficient of the air gap, kg/(m² Pa h)
c_k	—	Membrane coefficient based on the Knudsen diffusion model, kg/(m² Pa h)
c_m	—	Mass transfer coefficient of membrane, kg/(m² Pa h)
D_c	—	Diameter of the cold side channel, m
D_h	—	Diameter of the hot side channel, m
D_m	—	Diffusion coefficient of air and vapor in the membrane, m²/s
d_h	—	Hydraulic diameter of the empty channel
f_F	—	Fanning friction factor
g	—	Gravity
H_{lost}	—	Total power consumption due to hydraulic loss of both cold and hot channel
H_m	—	Membrane heat transfer coefficient
h	—	Convection coefficient, $W/(m^2 K)$
h_f	—	Convection coefficient of the condensation layer, W/(m² K)
H_{lost}	—	Total hydraulic loss of the AGMD system, J/s
I_N	—	Permeate flux increment
I_P	—	Energy consumption increment
k_a	—	Thermal conductivity coefficient of the air, W/(mK)
k_f	—	Thermal conductivity coefficient of the fluid, W/(mK)
k_g	—	Thermal conductivity of the gas in the pore of the membrane, W/(mK)
k_m	—	Thermal conductivity of membrane, W/(mK)
k_p	—	Thermal conductivity of aluminum plate, W/(mK)
L	—	Equivalent channel length, m
ℓw_f	—	Friction loss factor, J/kg
M_w	—	Molecular weight of water vapor, kg/mol
$\dot{m}$	—	Mass flow rate, kg/s
Nu	—	Nusselt number
N''_a	—	Membrane flux of the air gap, kg/(m² h)
N''_m	—	Membrane flux, kg/(m² h)
N_s	—	Membrane flux of the AGMD with helical wired channel, kg/(m² h)
P	—	Pressure, Pa
P_1	—	Saturated vapor pressure of water on the hot side surface of membrane, Pa
P_2	—	Saturated vapor pressure of water on the air gap side surface of membrane, Pa
P_3	—	Saturated vapor pressure of water in the air gap, Pa
P_w	—	Saturated vapor pressure of water, Pa
Pr	—	Prandtl number
Q	—	Volumetric flow rate, m³/s
q_h	—	Heat transfer rate of the hot feed fluid to the membrane surface, W/m²
q_m	—	Heat transfer rate of the membrane, W/m²
q_a	—	Heat transfer rate of the membrane surface to air gap, W/m²
q_f	—	Heat transfer rate of the condensation layer to the metal plate surface, W/m²
q_p	—	Heat transfer rate of the metal plate, W/m²
q_c	—	Heat transfer rate of the metal plate surface to the cold side, W/m²
R	—	Gas constant, J/mol K
Re	—	Reynolds number
r	—	Radius of membrane pore, m
T	—	Temperature, °C
T_h	—	Bulk fluid temperature of the hot feed side, °C
T_1	—	Temperature of the membrane surface on the hot side, °C
T_2	—	Temperature of the membrane surface on the air gap side, °C
T_3	—	Temperature on the condensation layer, °C
T_4	—	Temperature of the metal surface on the condensation layer side, °C
T_5	—	Temperature of the metal surface on the cold fluid side, °C
T_c	—	Bulk fluid temperature of the cold side, °C
TPC	—	Temperature polarization coefficient
u	—	Average velocity of the fluid, m/s
$\overline{v}$	—	Average velocity in the stream
W	—	Effective width of the channel, m
x_{NaCl}	—	Mole fraction of NaCl in saline solution
x_w	—	Mole fraction of water in saline water
Y_m	—	Natural log mean mole fraction of air
y_w	—	Vapor mole fraction of water
z	—	Axial coordinate along the flow direction, m

Greek

α^S	—	The enhancement factor of the heat transfer coefficient
δ_m	—	Thickness of membrane, m
δ_a	—	Thickness of the air gap, m
δ_p	—	Thickness of the metal plate, m
ε	—	Membrane porosity
λ	—	Latent heat of water, J/kg
ρ	—	Density, kg/m^3
τ_{temp}	—	Temperature polarization coefficient
μ	—	Viscosity of the fluid, N s/m^2

Subscripts

c	—	Cold fluid
h	—	Hot fluid

Acknowledgment

The authors wish to thank the Ministry of Science and Technology of the Republic of China (Taiwan) for the financial support.

References

[1] F.A. Banat, J. Simandi, Theoretical and experimental study in membrane distillation, Desalination, 95 (1994) 39–52.
[2] S. Bandini, G.C. Sarti, Heat and ass transport resistances in membrane distillation per drop, J. Membr. Sci., 45 (1999) 1422–33.
[3] O. Miyatake, H. Iwashita, Laminar-flow heat transfer to a fluid flowing axially between cylinders with a uniform wall heat flux, Int. J. Heat Mass Transfer, 34 (1991) 322–327.
[4] U. Dehesa-Carrasco, C.A. Perez-Rabago, C.A. Arancibia-Bulnes, Experimental evaluation and modeling of internal temperatures in an air gap membrane distillation unit, Desalination, 326 (2013) 47–54.
[5] A. Alkhudhiri, N. Hilal, Air gap membrane distillation: a detailed study of high saline solution, Desalination, 423 (2017) 179–86.
[6] K.W. Lawson, D.R. Lloyd, Membrane distillation, J. Membr. Sci., 124 (1997) 1–25.
[7] M. Gryta, M. Tomaszewska, J. Grzechulska, A.W. Morawski, Membrane distillation of NaCl solution containing natural organic matter, J. Membr. Sci., 181 (2001) 279–287.
[8] E. Drioli, A. Ali, F. Macedonio, Membrane distillation: recent developments and perspectives, Desalination, 356 (2015) 56–84.
[9] Y.C. Woo, L.D. Tijing, W.G. Shim, J.S. Choi, S.H. Kim, T. He, E. Drioli, H.K. Shon, Water desalination using graphene-enhanced electro spun nanofiber membrane via air gap membrane distillation, J. Membr. Sci., 520 (2016) 99–110.
[10] A. Khalifa, D. Lawal, M. Antar, M. Khayet, Experimental and theoretical investigation on water desalination using air gap membrane distillation, Desalination, 376 (2015) 94–108.
[11] L. García-Fernández, B. Wang, M.C. García-Payo, K. Lib, M. Khayet, Morphological design of alumina hollow fiber membranes for desalination by air gap membrane distillation, Desalination, 420 (2017) 226–240.
[12] A.E. Khalifa, S.M. Alawad, Air gap and water gap multistage membrane distillation for water desalination, Desalination, 437 (2018) 175–183.
[13] H.C. Duong, M. Duke, S. Gray, P. Cooper, L.D. Nghiem, Membrane scaling and prevention techniques during seawater desalination by air gap membrane distillation, Desalination, 397 (2016) 92–100.
[14] A. Alkhudhiri, N. Darwish, N. Hilal, Membrane distillation: a compressive review, Desalination, 287 (2012) 2–18.
[15] M.E. Findley, Vaporization through porous membranes, Ind. Eng. Chem. Process Des. Dev., 6 (1967) 226–230.
[16] Y. Henderyckx, Evaporation-Condensation Recovery of a Solution Component Using Vapor-per-Meable Wall Spaced from a Cold Wall, US Patent 3563860 A, United States Patent Office, 1971.
[17] J. Koschikowski, M. Wieghaus, M. Rommei, Solar thermal-driven desalination plants based on membrane distillation, Desalination, 156 (2003) 295–304.
[18] K. Yao, Y. Qin, Y. Yuan, L. Liu, F. He, Y. Wu, A continuous-effect membrane distillation process based on hollow fiber AGMD module with internal latent-heat recovery, AIChE J., 59 (2013) 1278–1297.
[19] C.M. Guijt, G.W. Meindersma, T. Reith, A.B. de Haan, Air gap membrane distillation: 2. Model validation and hollow fiber module analysis, Sep. Purif. Technol., 43 (2005) 245–255.
[20] B.G. Im, J.G. Lee, Y.D. Kim, W.S. Kim, Theoretical modeling and simulation of AGMD and LGMD desalination processes using a composite membrane, J. Membr. Sci., 565 (2018) 14–24.
[21] S. Al-Obaidani, E. Curcio, F. Macedonio, G.D. Profio, H. Al-Hinai, E. Drioli, Potential of membrane distillation in seawater desalination: thermal efficiency, sensitivity study and cost estimation, J. Membr. Sci., 323 (2008) 85–98.
[22] R.W. Schofield, A.G. Fane, C.J.D. Fell, Heat and mass transfer in membrane distillation, J. Membr. Sci., 33 (1987) 299–313.
[23] L. Martínez-Díez, M.I. Vázquez-González, Effects of polarization on mass transport through hydrophobic porous membranes, Ind. Eng. Chem. Res., 37 (1998) 4128–4135.
[24] A. Ruiz-Aguirre, J.A. Andrés-Mañas, J.M. Fernández-Sevilla, G. Zaragoza, Experimental characterization and optimization of multi-channel spiral wound air gap membrane distillation modules for seawater desalination, Sep. Purif. Technol., 205 (2018) 212–222.
[25] R. Bahar, M.N.A. Hawlader, T.F. Ariff, Channeled coolant plate: a new method to enhance freshwater production from an air gap membrane distillation (AGMD) desalination unit, Desalination, 359 (2015) 71–81.
[26] X. Yang, H. Yu, R. Wang, A.G. Fane, Analysis of the effect of turbulence promoters in hollow fiber membrane distillation modules by computational fluid dynamic (CFD) simulations, J. Membr. Sci., 415–416 (2012) 758–769.
[27] T. Wang, Z. Zhang, X. Ren, L. Qin, D. Zheng, J. Li, Direct observation of single- and two-phase flows in spacer filled membrane modules, Sep. Purif. Technol., 125 (2014) 275–283.
[28] L.H. Cheng, Y.H. Lin, J.H. Chen, Enhanced air gap membrane desalination by novel finned tubular membrane modules, J. Membr. Sci., 378 (2011) 398–406.
[29] C.D. Ho, H. Chang, C.L. Chang, C.H. Huang, Theoretical and experimental studies of flux enhancement with roughened surface in direct contact membrane distillation desalination, J. Membr. Sci., 433 (2013) 160–166.
[30] H.M. Yeh, Enrichment of heavy water in rotated wired concentric-tube thermal diffusion columns, Sep. Purif. Technol., 40 (2004) 321–325.
[31] A.S. Jönsson, R. Wimmerstedt, A.C. Harrysson, Membrane distillation - a theoretical study of evaporation through microporous membranes, Desalination, 56 (1985) 237–249.
[32] A.S. Alsaadi, N. Ghaffour, J.D. Li, S. Gray, L. Francis, H. Maab, G.L. Amy, Modelling of air-gap membrane distillation process: a theoretical and experimental study, J. Membr. Sci., 445 (2013) 53–65.
[33] F.A. Banat, J. Simandl, Membrane distillation for dilute ethanol Separation from aqueous streams, J. Membr. Sci., 163 (1999) 333–348.
[34] H.M. Yeh, H.C. Ward, The improvement in separation concentric-tube thermal diffusion column, Chem. Eng. Sci., 26 (1971) 937–947.
[35] T.A. Washall, F.W. Melpolder, Improving the separation efficiency of liquid thermal diffusion columns, Ind. Eng. Chem. Process Des. Dev., 1 (1962) 26–28.
[36] H. Geng, H. Wu, P. Li, Q. He, Study on a new air-gap membrane distillation module for distillation, Desalination, 334 (2014) 29–38.

[37] P. Poskas, V. Simonis, Heat transfer in initial part of thermal stabilization of helical channels in air flow, Heat Transfer Res., 43 (2012) 443–460.
[38] G.L. Liu, C. Zhu, C.S. Cheung, C.W. Leung, Theoretical and experimental studies on air gap membrane distillation, Heat Mass Transfer, 34 (1998) 329–335.
[39] M.A. Izquierdo-Gil, M.C. García-Payo, C. Fernández-Pineda, Air gap membrane distillation of aqueous alcohol solutions, J. Membr. Sci., 169 (2000) 61–80.
[40] S.B. Warner, Fiber Science, Princeton-Hall, Englewood Cliffs, NJ, 1995.
[41] K.W. Lawson, D.R. Lloyd, Membrane distillation, J. Membr. Sci., 124 (1997) 1–25.
[42] R.W. Schofield, A.G. Fane, C.J.D. Fell, Gas and vapor transport through microporous membranes, I. Knudsen-Poiseuille transition, J. Membr. Sci., 53 (1990) 159–171.
[43] J. Phattaranawik, R. Jiraratananon, A.G. Fane, Heat transport and membrane distillation coefficient in direct contact membrane distillation, J. Membr. Sci., 212 (2002) 177–193.
[44] S.G. Kandlikar, D. Schmitt, Characterization of surface roughness effects on pressure drop in single-phase flow in minichannels, Phys. Fluids, 17 (2005) 100606–100606–11, doi: 10.1063/1.1896985.
[45] H.M. Yeh, F.K. Ho, A study of the separation efficiency of wired thermal diffusion columns with tubes rotating in opposite directions, Chem. Eng. Sci., 75 (1975) 1381–1385.
[46] C.D. Ho, L. Chen, F.C. Tsai, G.H. Lin, J.W. Lim, Distillate flux enhancement of the concentric circular direct contact membrane distillation module with spiral wired flow channel, J. Taiwan Inst. Chem. Eng., 94 (2019) 70–80.
[47] H. Chang, C.Y. Hung, C.L. Chang, T.W. Cheng, C.D. Ho, Optimization of three small-scale solar membrane distillation desalination systems, Membr. Water Treat., 6 (2015) 451–476.